RESEARCH ARTICLE

VOLCANICA

# Accurate hindcasting of explosive eruptions at Whakaari, New Zealand: banded tremor precursors for future forecasts

John Stix*[α], Craig Miller[β], and Yajing Liu[α]

[α] Department of Earth and Planetary Sciences, McGill University, 3450 University Street, Montreal, Quebec H3A 0E8, Canada.
[β] GNS Science Te Pū Ao, 114 Karetoto Road, RD4, Taupō 3384, New Zealand.

## Abstract

Phreatic eruptions are small, sudden events, commonly with few precursory signals. They are driven by interactions between magmatic and hydrothermal processes at shallow levels beneath the surface. Here we show that a sequence of banded tremor events, which occurred several weeks before the 9 December 2019 eruption of Whakaari (White Island), New Zealand, can be used to hindcast this eruption. The banded tremor sequence reveals a progressively decreasing time interval between tremor bands. Extrapolating the tremor bands to a time interval of zero provides an accurate estimate, at least one week prior to the eruption, to within 10.2 hours of when the eruption would occur, with a 2.8-day range between 95 % confidence intervals. A similar set of tremor signals appeared before the 27 April 2016 eruption, and these signals provide a very accurate hindcast of this eruption to within 2.61 hours, with a 2.2-day range between 95 % confidence intervals. Our analysis indicates that this potential forecasting approach may prove useful for successfully and accurately forecasting future eruptions at Whakaari. The approach also may be applicable to other volcanoes similar to Whakaari which experience sudden phreatic and phreatomagmatic eruptions.

Keywords: Phreatic eruptions; Whakaari volcano; Banded tremor; Eruption forecasting.

Submitted: 2023-03-26 | Accepted: 2023-12-21 | Published: 2024-03-11

Editor: C. Caudron | Typesetter: E.C. Hughes

## 1 Introduction

Phreatic eruptions are common events globally [Barberi et al. 1992]. Due to complex feedbacks between subsurface magmatic and hydrothermal processes [Stix and de Moor 2018; Montanaro et al. 2022], we lack insight regarding mechanisms, triggers, and impending signs of these eruptions. Because of their sudden nature, phreatic eruptions can be lethal to people in the vicinity of active craters, as has recently occurred at Ontake in Japan [Yamaoka et al. 2016] and at Whakaari (White Island) in New Zealand [Kilgour et al. 2021]. No phreatic eruption has yet been successfully forecast, although recent advances have been made at Whakaari using a number of approaches including inverse Real-time Seismic Amplitude Measurement [RSAM; Chardot et al. 2015], machine learning [Dempsey et al. 2020], and normalized Displacement Seismic Amplitude Ratios [nDSAR; Ardid et al. 2022].

A key problem for these types of events is the lack of precursory signals before an eruption. This is probably the main reason why forecasting such events in real time has not been successful to date. For an eruption precursor to be useful for forecasting, it needs to occur reliably before eruptions, and not occur during times of repose [Ardid et al. 2022; Dempsey et al. 2022]. If the precursors are unreliable, then eruptions may be missed. If such signals occur during repose, false positives will ensue. The issue is complicated and complex, because when phreatic systems pressurize, the pressurization sequence may or may not end in eruption. In other words, sometimes the system stops short of erupting. In this paper we examine an eruption precursor – banded tremor – which can be reliably used to hindcast two eruptions of Whakaari.

Whakaari is a mostly submarine volcano of andesitic to dacitic composition [Figure 1; Cole et al. 2000]. It is New Zealand's most active volcano, with a high degree of unrest and frequent small eruptions [Kilgour et al. 2021]. Styles of eruptive activity include Strombolian, phreatomagmatic, and phreatic due to variable interactions between magma and external water [Houghton and Nairn 1991; Kilgour et al. 2021]. The volcano's activity is the result of a complex interplay between a shallow hydrothermal system and a shallow magmatic system beneath the active crater area [Christenson et al. 2017]. This interplay makes the volcano an ideal natural laboratory to study magmatic-hydrothermal processes. The hydrothermal system is characterized by spatially and temporally variable porosity, permeability, and mineralization including native sulphur, anhydrite, alunite, cristobalite, and albite [Kennedy et al. 2020]. The magmatic system also resides at shallow levels, with magma occasionally reaching the surface [Jolly et al. 2020].

Beginning in 2012, a series of phreatic and phreatomagmatic eruptions have taken place periodically at Whakaari. These eruptions are sudden, with few apparent precursors. The most recent eruption occurred on 9 December 2019, killing 22 people and seriously injuring a number of others who were visiting the island at the time. A series of unusual tremor spikes occurred in a regular fashion for several weeks prior to this eruption. This type of signal is termed banded tremor [Banks et al. 1989]; such signals have been used to indicate proximity to explosive phreatic eruptions at Karkar [McKee et al. 1981], Nevado del Ruiz [Martinelli 1990], and Etna [Gresta et al. 1996]. The primary goal of this paper is to examine this tremor sequence in detail, use it for hindcasting the eruption, and interpret its evolution to explain the behaviour of the volcano before, during, and after the eruption. We then search for similar tremor sequences from other eruptions of Whakaari, to see if these sequences could also be used for retrospective hindcasting purposes with the view to understanding a common causative mechanism across several eruptions.

* stix@eps.mcgill.ca

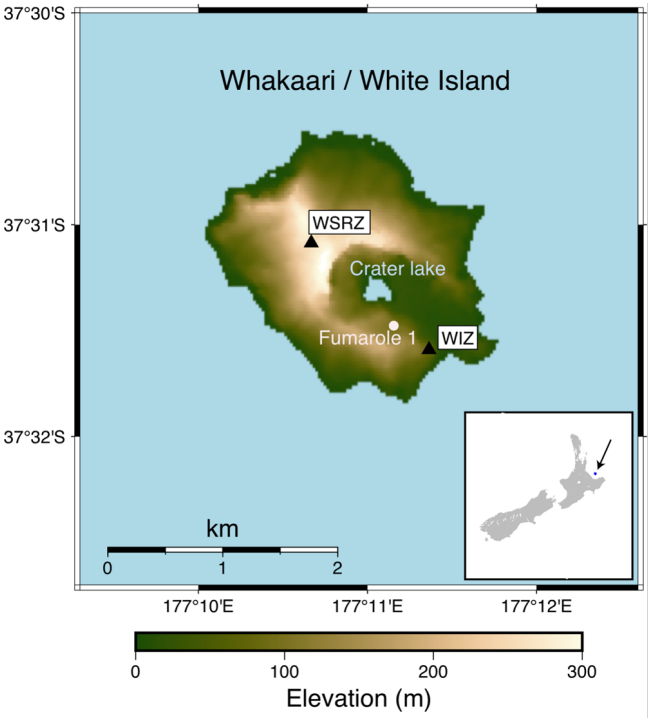


Figure 1: Locations of seismic stations WSRZ and WIZ, the crater lake/vent, and Fumarole 1 on Whakaari/White Island. Inset points to the location of Whakaari in New Zealand.

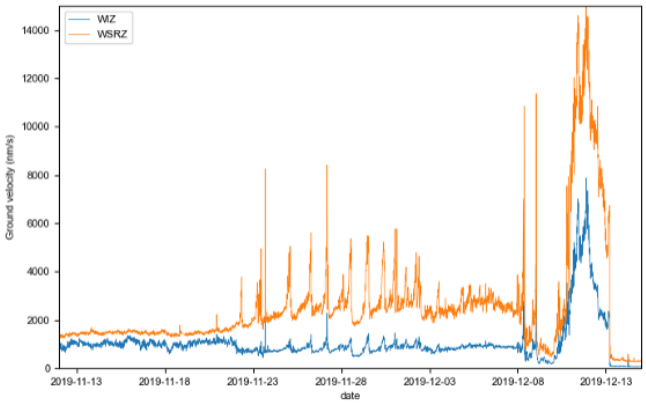


Figure 2: Ground velocities recorded by the WSRZ and WIZ seismic stations at Whakaari in November and December 2019. Data are 10-minute, 2–5 Hz-filtered RSAM.

## 2 Determination of tremor band intervals

A sequence of unusual tremor signals was recorded at Whakaari beginning on 22 November 2019 [GeoNet 2019b], 17 days before the 9 December eruption. These signals were recorded on both the WSRZ and WIZ seismic stations on the island [Figure 1; GNS Science 2021]. However, the closer proximity of WSRZ to the crater meant the signal to noise ratio is higher at that station (Figure 2). Hence we use data from WSRZ in our analysis. We use 10-minute RSAM data which were 2–5 Hz-filtered to remove the higher frequency component typically caused by wind. Since wind is usually a broadband signal, the bandpass filtering removes the majority of the wind signal. Other signals, such as those generated by sightseeing helicopters, generate a distinctive waveform with a duration of only several minutes during daylight hours. Thus, within 10-minute RSAM data, helicopter interference would not occupy more than one or two 10-minute readings (maximum). Furthermore, Meng and Ben-Zion [2018] show that the average duration of aircraft noise transiting a seismometer array in California is about 200 s and exhibits distinctive high frequency (>50 Hz) signals which are well above the frequency of interest and indeed above the Nyquist frequency of the seismic station sampling rate at 100 Hz.

At Whakaari, the tremor bands were well defined from 22 November until 2 December 2019 (Figure 3A). These bands were recognized by Ardid et al. [2022] and interpreted as pulsating gas fluxes. Thereafter, the amplitudes of the bands declined from 2 to 6 December, although they are still recognizable (Figure 3B). By December 7–8, the tremor signal was small without recognizable bands. During this period, the low-level tremor was interrupted by two large tremor spikes at 17.5 and 16.2 hours before the eruption which occurred on 9 December at 1411 hours local time (0111 hours UTC). These tremor spikes were observed and reported as a precursor by Dempsey et al. [2020]. After the eruption, tremor continued at low levels for about a day before ramping up rapidly to very high levels in the following three days [Dempsey et al. 2022].

We first visually identified the tremor bands and intervals from the published GeoNet data at WSRZ [GeoNet 2019b], then we used the 10-minute RSAM data for detailed analysis. The principal criterion for identifying and selecting a tremor band is that the band is clearly identifiable and distinguishable from the background, based on visual inspection and further verified numerically. The bands and time intervals between each band were then measured manually (Table 1). We place particular emphasis on the data from 22 November to 2 December 2019 (Figure 3A) because these tremor bands are prominent, well developed, and clearly distinguishable from the background. Another interesting characteristic of most tremor bands during this period is a gradual increase in amplitude over the course of hours to the maximum value of the tremor band, followed by a rapid decline in amplitude. The peak observed within interval #5 (Figure 3A) is considered to be part of the gradual increase to the subsequent tremor band, hence was not selected as a separate tremor band based on visual inspection and further numerical verification. A regional earthquake occurs within interval #2, and this event was removed from consideration when identifying the tremor bands. The timing of a particular tremor band (and thus the time interval between successive bands) was determined by its maximum amplitude, except for the band at the beginning of interval #9 and the band at the end of interval #10. These two bands have prominent doublet spikes, and their timing was determined to be halfway between the doublet spikes.

For the time period of 2–6 December 2019, the overall amplitudes of the tremor bands are substantially reduced when compared to 22 November to 2 December (Figure 3B). Of the 13 tremor bands identified during 2–6 December, the majority stand out from the background, while 3–4 bands are less prominent. Hence there is some subjectivity in choosing tremor peaks for this time period, and these time interval data may be less reliable.

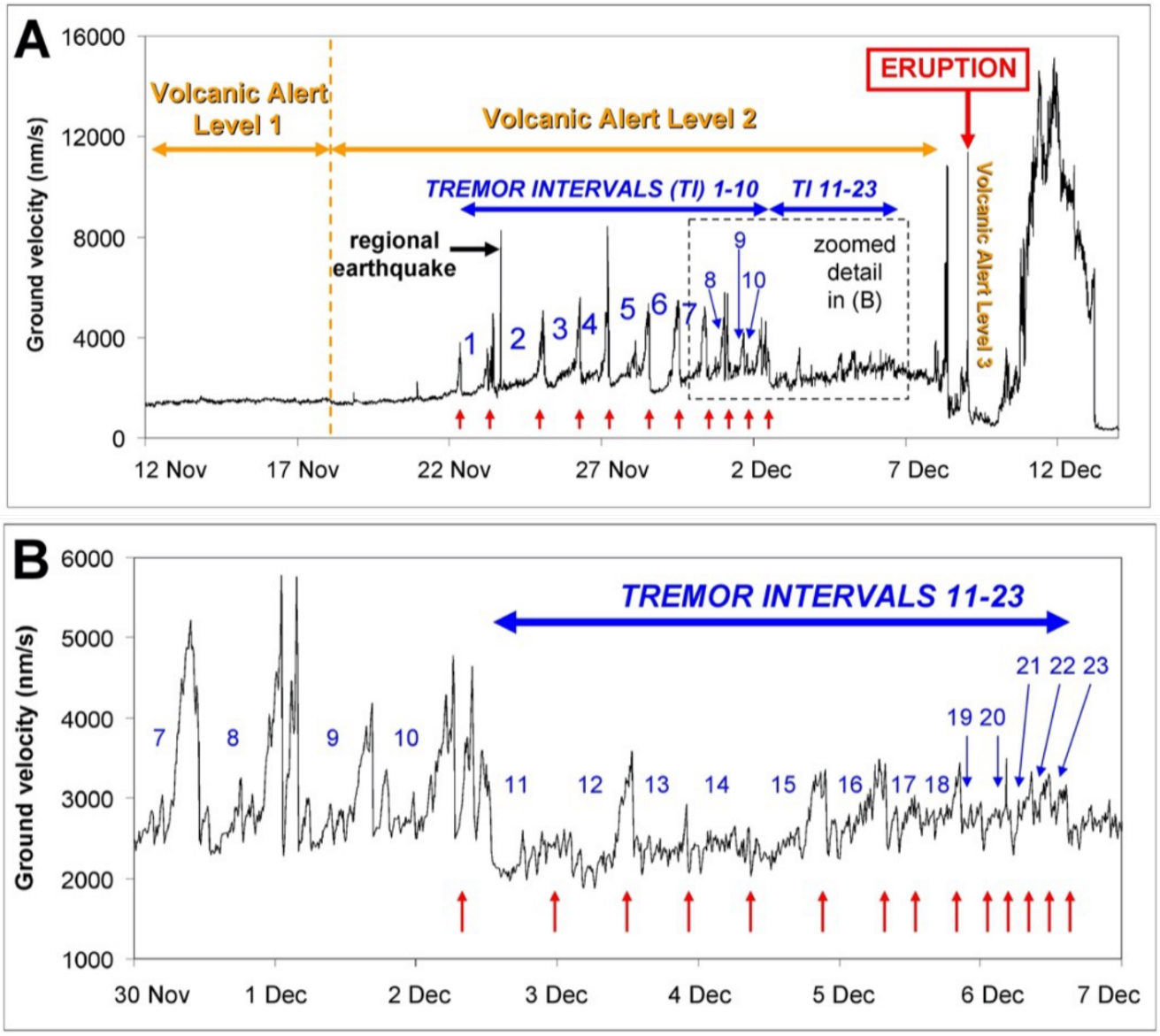


Figure 3: [A] Ground velocity recorded by the WSRZ seismic station at Whakaari for one month from 12 November to 14 December 2019. Data are 10-minute, 2–5 Hz-filtered RSAM. Tremor intervals for intervals #1–10 are numbered. Vertical red arrows show tremor peaks. Elevated levels of tremor began on 22 November, soon after a change in the Volcanic Alert Level from 1 to 2. Tremor bands were distinct from 22 November to 2 December (tremor bands #1–10), and less pronounced during 2–6 December (tremor bands #11–23). Thereafter, the tremor level was comparatively low from 6 December until the eruption on 9 December, punctuated by one small and one large tremor spike at 17.5 and 16.2 hours, respectively, prior to the eruption. After the eruption, tremor was low for about a day before increasing rapidly to very high levels for about three days. [B] Numbering of tremor intervals for intervals #11–23. Vertical red arrows show tremor peaks.

Since the peaks were initially chosen by visual inspection, we also used two peak detection algorithms to compare and validate the manually picked results with a view to being able to automate the procedure. The first algorithm uses a critical ground velocity $V_{cr}$ to identify separate periods of high velocities. Within each period, if there are multiple peak velocities offset by no more than a critical duration $T_{cr}$, they are grouped as a single peak at the occurrence time of the highest velocity. Figure 4A shows that between 22 November and 2 December, by manually selecting $V_{cr} = 3250\,\mathrm{nm\,s^{-1}}$ and $T_{cr} = 0.3$ days, we can identify 12 peak occurrences and the successive intervals. Between 3–7 December we used $V_{cr} = 2850\,\mathrm{nm\,s^{-1}}$ and $T_{cr} = 0.2$ days to account for the lower peak velocities and more frequent occurrences. Using slightly different choices of $V_{cr}$ and $T_{cr}$ from the above values, as long as they can reasonably differentiate velocity peaks from troughs, results in identical or nearly identical sets of intervals.

For the second method we calculated the STA/LTA ratio (short-term average versus long-term average) which takes two continuously sliding time windows of the RSAM time series, with the shorter time window representing the current shaking and the longer window representing the background noise level and identified peak occurrence times and intervals. Figure 4B shows the 12 peaks identified between 22

Table 1: Time data for intervals #1–23, 2019.

| Interval | Interval time (days) | Elapsed time since 0830 hrs UTC, 22 Nov 2019 (days) |
|---|---|---|
| 1 | 1.097 | 1.097 |
| 2 | 1.646 | 2.743 |
| 3 | 1.194 | 3.937 |
| 4 | 0.917 | 4.854 |
| 5 | 1.340 | 6.194 |
| 6 | 0.979 | 7.174 |
| 7 | 0.875 | 8.049 |
| 8 | 0.694 | 8.743 |
| 9 | 0.590 | 9.333 |
| 10 | 0.642 | 9.976 |
| 11 | 0.594 | 10.569 |
| 12 | 0.604 | 11.174 |
| 13 | 0.389 | 11.562 |
| 14 | 0.444 | 12.007 |
| 15 | 0.542 | 12.549 |
| 16 | 0.382 | 12.931 |
| 17 | 0.250 | 13.181 |
| 18 | 0.319 | 13.500 |
| 19 | 0.153 | 13.653 |
| 20 | 0.174 | 13.826 |
| 21 | 0.181 | 14.007 |
| 22 | 0.125 | 14.132 |
| 23 | 0.118 | 14.250 |

November and 2 December by using a short-term time window of 0.1 days, a long-term time window of 0.5 days, and a STA/LTA cutoff ratio of 0.5. As with the $V_{cr}/T_{cr}$ algorithm, small variations in the STA, LTA time windows and the cutoff ratio would not significantly change the timing and interval of the peaks. We did not extend the STA/LTA analysis after 2 December, since the ratio fluctuates around 0.5 without clear peaks after this date. The STA/LTA smoothing also results in slight phase shifts in the timing of identified peaks, in particular when there are closely spaced RSAM peaks (Figure 4B).

Unlike the manual picks, both algorithms identified #5 as a separate interval as it satisfies the prescribed selection criteria. Figure 4C shows that, regardless of the peak identification methods (manual or automatic), the overall trend of decreasing intervals approaching the eruption is robust. The only clear outlier is the long interval of ~1.5 days on 4 December (purple circle, Figure 4C), because with the prescribed $V_{cr}$ and $T_{cr}$ the algorithm cannot differentiate the subtle peaks between 2–4 December. We acknowledge that both algorithms are dependent on certain *a-priori* information such as the range of the RSAM amplitude in each cycle, at least for the first few intervals, to choose the thresholds. Furthermore, as the volcanic system develops in the pre-eruption period, these banded tremor patterns may correspondingly evolve and thus require adaptive thresholds. Real-time or near real-time data access and analysis are critical for this approach to be practical in future forecasting tools.

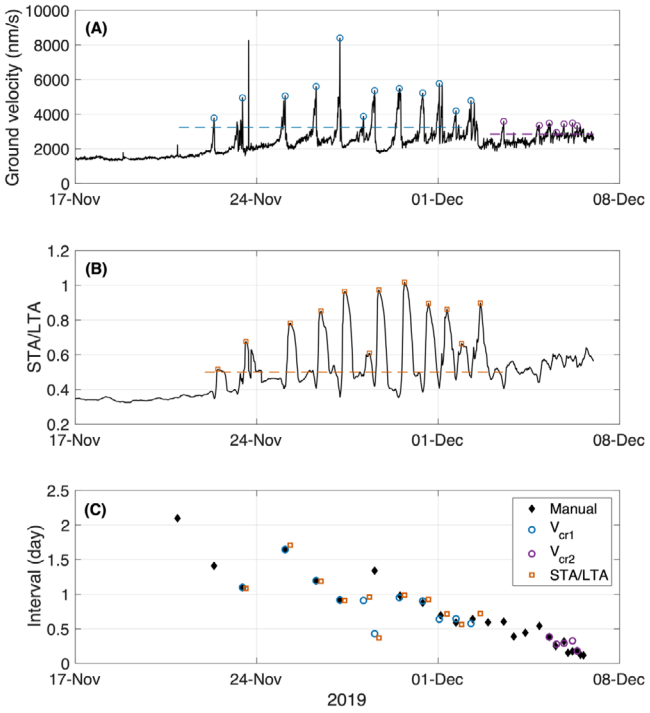


Figure 4: [A] Tremor bands selected by applying $V_{cr}$ = 3250 nm s$^{-1}$, $T_{cr}$ = 0.3 days (blue circles) between 22 November and 2 December, and $V_{cr}$ = 2850 nm s$^{-1}$, $T_{cr}$ = 0.2 days (purple circles) between 3–7 December, to the RSAM velocity, [B] tremor bands selected by STA/LTA using short-term window of 0.1 days and long-term window of 0.5 days and a cutoff STA/LTA ratio of 0.5 (orange squares) between 22 November and 2 December, and [C] comparison of tremor band intervals identified from visual inspection (black diamonds, same as in Figure 5), from RSAM raw data (blue and purple circles) and from STA/LTA ratio (orange squares).

## 3 Hindcasting the 9 December 2019 eruption of Whakaari

We now analyze the pre-eruption tremor data to calculate a hindcast of when the 9 December 2019 eruption should have occurred. With the benefit of hindsight, it may have been possible to forecast this eruption. From 22 November until 6 December, we visually identified 23 intervals of comparatively low-level tremor between each tremor band (Figure 3). The durations of these intervals vary with time, from ~26–40 hours at the beginning of the sequence on 22 November to less than 5 hours near the end of the sequence on 6 December. In detail, the durations exhibit a systematic, quasi-linear decrease with time (Table 1). In Figure 5, we plot these time intervals as a function of time in days to the eruption at 0111 hours UTC on 9 December 2019. Using a linear fit to the data, it is possible to extrapolate this trend to $y = 0$, i.e. the point at which the intervals become zero. The extrapolation yields 16.27 days from the initial tremor band at 0830 hours UTC on 22 November, with the 95 % confidence intervals at 15.15 and 17.93 days, respectively, hence a range of 2.78 days. This "zero point" is 10.2 hours before the eruption on 9 December which occurred 16.69 days after the initial tremor band. Hence this approach provides an accurate hindcast for the date of the eruption. The

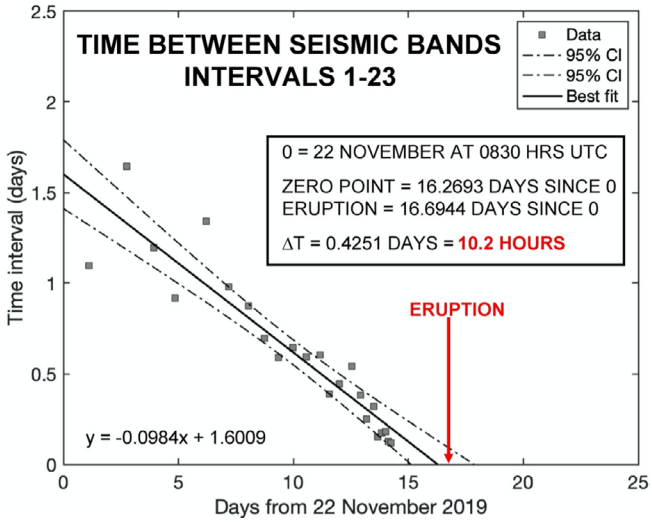


Figure 5: Duration of time intervals between tremor bands plotted from 22 November to 6 December 2019. Extrapolation of the time interval to zero gives an elapsed time of 16.27 days since 0830 hours UTC on 22 November. This elapsed time corresponds to 14:59 hours UTC on 8 December. The eruption occurred at 0111 hours UTC on 9 December, 10.2 hours (ΔT) after the hindcasted time. The 95 % confidence intervals at the extrapolated time ($y$ = 0) span 2.78 days.

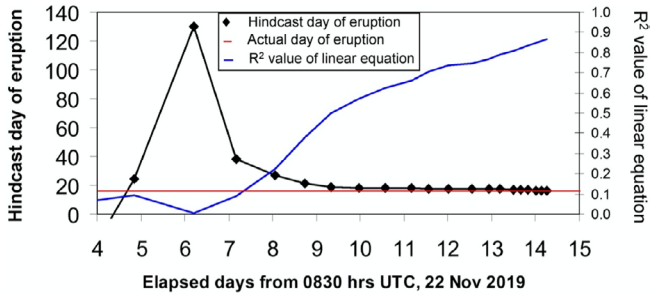


Figure 6: Plot showing hindcast day of eruption by extrapolating linear equations forward to where $y$ = 0 (the zero point). On the diagram, successive linear equations are constructed for cumulative time intervals between tremor bands, and the associated hindcast day of eruption is plotted (black diamonds). The horizontal red line shows the actual day of eruption (16.69 days) since the appearance of the first tremor peak at 0830 hours UTC on 22 November 2019. The blue line shows the changing $R^2$ values of the successive linear equations. The plot shows that by Day 9 (1 December), the hindcast days are approximating well the actual day of eruption, remaining stable through Day 14 (6 December).

algorithm-detected peak velocity times and intervals (Figure 4) are consistent with the linear trend established by the visual inspection data points (Figure 5).

A further analysis of the data can be made by examining the changing linear equations and zero points as each new tremor band forms in the sequence (Figure 6). By Day 9 (1 December), the hindcast days are approaching the actual day of the eruption, which occurred 16.69 days after the first tremor peak on 22 November at 0830 hours. From Day 9 and thereafter,

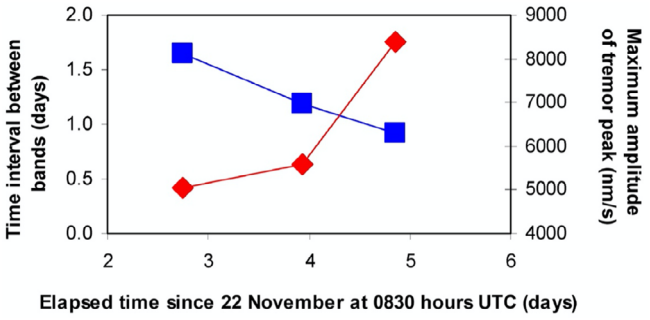


Figure 7: Fluctuations in time intervals between tremor bands and maximum amplitudes of tremor bands during the early stages of the tremor sequence. During intervals #2–4, time intervals decrease while maximum amplitudes increase.

the hindcast values are stable, thus accurate for determining when the eruption would occur. When we average these stable hindcast values over tremor intervals #9 to #23, the mean hindcast value is 17.27 days with a 95 % confidence limit of 1.3 days. This mean hindcast value is 13.8 hours after the eruption. Thus the "zero point" approach and hindcast averaging approach are both highly accurate with errors of 1–3 days.

The simple linear approach we have used is justified by the generally consistent zero point values. Nevertheless, the relationships that we have shown above may not be truly linear. For example, intervals #2–4 exhibit variability which could be a series of fluctuations (Figure 5). To illustrate this point, these intervals exhibit two tendencies, the first progressively shorter time intervals and the second progressively increasing maximum amplitudes of tremor bands (Figure 7). Thereafter, the fluctuating behaviour declines, and the trend toward zero becomes more stable and more linear with time. We discuss the implications of this behaviour below.

## 4 Hindcasting the 27 April 2016 eruption of Whakaari

We searched for similar signals before other eruptions at Whakaari since the current unrest and eruption sequence began in 2012. No clear banded tremor signals were observed prior to eruptions in August 2012, August 2013, and October 2013. Although there is an expression of banded tremor in October 2013, the peaks and intervals are too poorly defined for analysis. By contrast, a series of interesting tremor signals were noted before the 27 April 2016 eruption. These signals appear to begin on 17 April at 1410 hours UTC; they may in fact begin before this time, but the peaks are small and not clearly expressed in the RSAM data (Figure 8). From 17 to 24 April 2016, a series of four peaks occur which are shown in Figure 8A. Within this sequence, a peak on 19 April at 2110 hours UTC is due to a local M3.3 earthquake rather than tremor, so it was excluded. Two small peaks on 20 April were also ignored due to their comparatively small amplitudes relative to the other peaks. A wide band of elevated tremor occurs on 23–24 April, creating some uncertainty in terms of the correct tremor peak to use. Nevertheless, for this wide band, the maximum amplitude on 23 April at 1930 hours UTC was used for consistency. Beginning on 24 April at 2130 hours UTC,

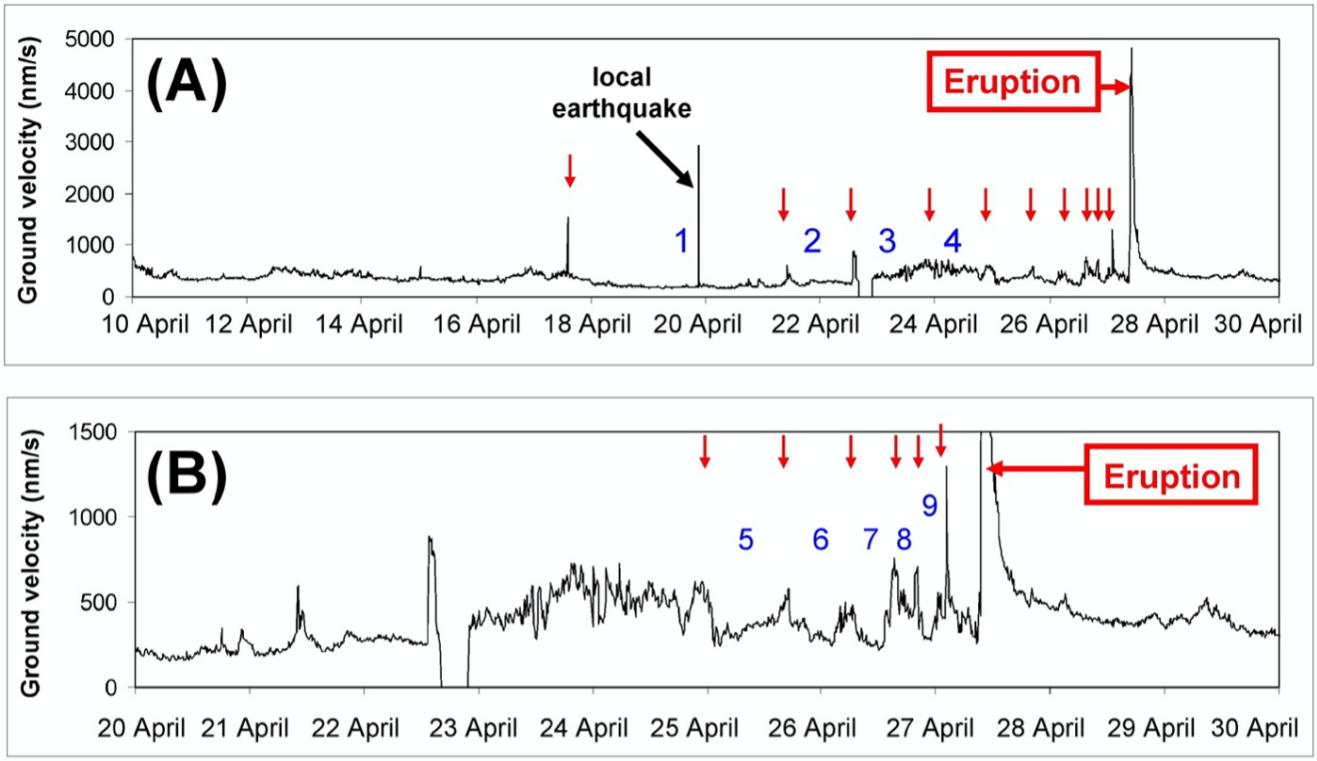


Figure 8: Ground velocity recorded by the WSRZ seismic station at Whakaari in April 2016 prior to an eruption on 27 April at 1020 hours UTC. Data are 10-minute, 2–5 Hz-filtered RSAM. [A] Ground velocity during 10–30 April. [B] Ground velocity during 20–30 April. A total of ten tremor peaks were observed from 17–27 April, with the last six peaks the most prominent. The vertical red arrows show tremor peaks, and the blue numbers indicate tremor intervals.

a further series of six peaks are well expressed (Figure 8B). Thus, there are ten peaks from 17 until 27 April at 0220 hours UTC, eight hours before the eruption at 1020 hours UTC. The time intervals between these peaks also decrease with time (Figure 9 and Table 2), similar to that seen for the 2019 data.

Treating the 2016 data in a similar fashion to the 2019 sequence and using all peaks and intervals, extrapolation of the time interval to zero gives an elapsed time of 9.64 days since the first peak, with the 95 % confidence intervals at 8.48 days and 12.42 days, respectively, hence a range of 3.94 days (Figure 9A). This extrapolation is 4.74 hours before the eruption. Using only the last six peaks, which are the best data, produces a zero point of 9.95 days, which is 2.61 hours after the eruption, with 95 % confidence intervals at 9.44 days and 11.67 days, respectively, thus a range of 2.23 days (Figure 9B). This hindcast can be made only 8.0 hours before the eruption. However, by neglecting the last peak on 27 April at 0220 hours UTC produces a zero point which is 2.328 hours before the eruption, and this hindcast can be made 14.2 hours before the eruption. These operational details may prove useful for future eruptions of Whakaari, in particular those where tremor peaks immediately precede an eruption and the time window for forecasting an eruption is short.

Table 2: Time data for intervals #1–9, 2016.

| Interval | Interval time (days) | Elapsed time since 1410 hrs UTC, 17 April 2016 (days) |
|---|---|---|
| 1 | 3.833 | 3.833 |
| 2 | 1.167 | 5.000 |
| 3 | 1.222 | 6.222 |
| 4 | 1.083 | 7.306 |
| 5 | 0.819 | 8.125 |
| 6 | 0.493 | 8.618 |
| 7 | 0.431 | 9.049 |
| 8 | 0.201 | 9.250 |
| 9 | 0.257 | 9.507 |

We did a further analysis of how the linear equations and zero points changed as each new tremor peak formed in the sequence (Figure 10), similar to our treatment for the 2019 eruption (Figure 6). In this analysis, we used all peaks and intervals. For the April 2016 sequence, the zero points become increasingly accurate with time. For example, two days before the eruption, the hindcast is indicating an eruption to within 22 hours of when the actual eruption occurred.

Similar to our treatment of the 2019 data, we ran the 2016 data through both our peak detection algorithms (Figure 11). The algorithm has difficulty in defining the initial tremor peaks of the sequence because of high frequency oscillations and less obvious peaks. For the last five peaks between 25–27 April, however, the algorithm's peak selection is fully consistent with the peaks chosen by visual inspection and displays a linear decreasing trend of band intervals toward the eruption. Hence the two approaches accurately hindcast the eruption using these five peaks. In summary, our approach is able to

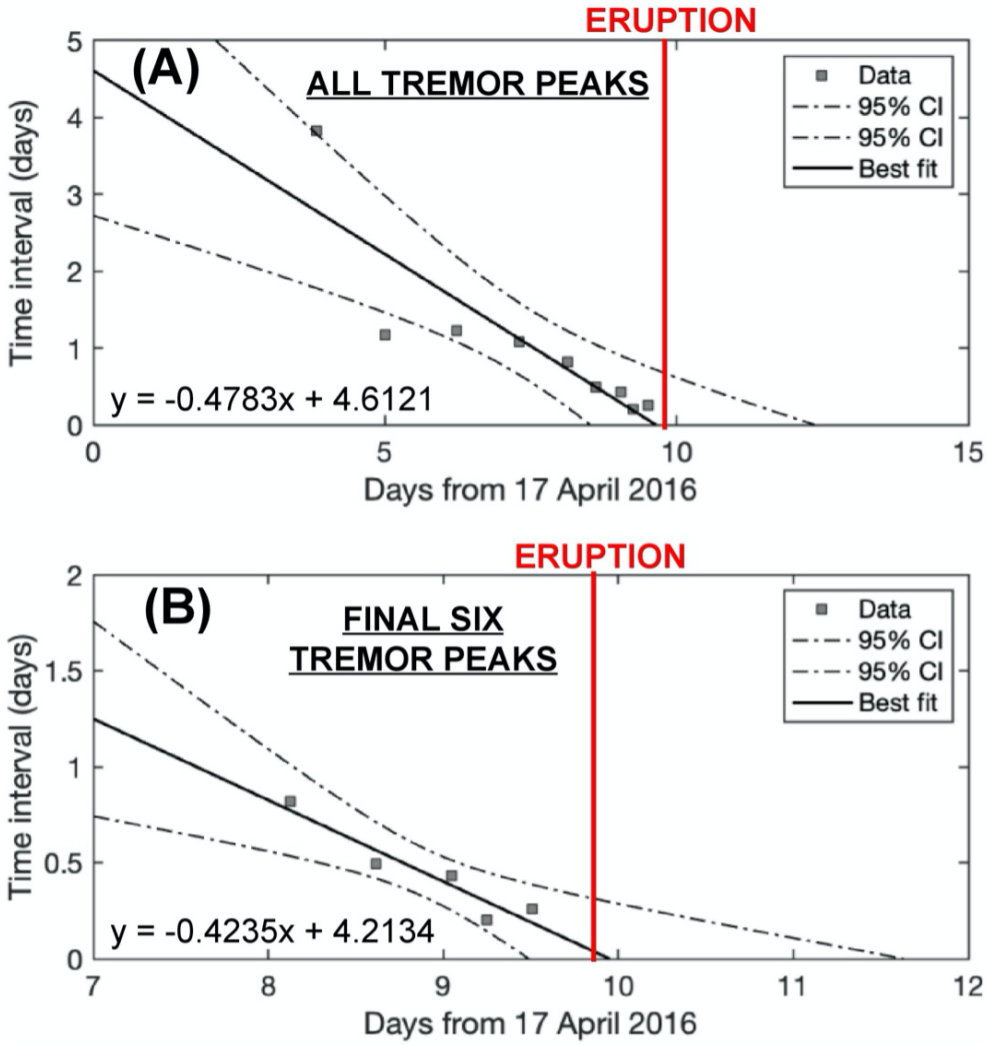


Figure 9: [A] Durations of time intervals between tremor peaks plotted from the first peak occurring on 17 April 2016 at 1410 hours UTC. Extrapolation of the time interval to zero gives an elapsed time of 9.64 days since the first peak. This zero point is 4.7 hours before the eruption at 1020 hours UTC on 27 April. The 95 % confidence intervals at the extrapolated time ($y$ = 0) span 3.94 days. [B] Same approach as in [A] above but using only the last six tremor peaks prior to the eruption. This zero point occurs 2.6 hours after the eruption. The 95 % confidence intervals at the extrapolated time ($y$ = 0) span 2.23 days.

hindcast the 2016 eruption at several different timescales, and it appears accurate to within several hours of the eruption.

## 5 Discussion

The pre-eruptive tremor that we have observed at Whakaari provides a means to accurately hindcast the two most recent eruptions. For the 2019 tremor sequence, the changing patterns of the tremor over several weeks' time can be related to subsurface processes within the volcano leading to its eruption. The occurrence of the tremor starting on 22 November is indicative of the interaction of the shallow magmatic system with the shallow hydrothermal system, whereby hot magmatic gas and possibly magma were injected into the hydrothermal system. We propose this injection caused the two-phase or liquid-dominated portion of the hydrothermal system [Miller et al. 2020] to boil periodically, creating the tremor signals.

Similar periodic tremor signals were noted by Vandemeulebrouck et al. [2005] at Inferno Crater, Waimangu geothermal field, New Zealand, who ascribed them to periodic boiling of the shallow hydrothermal system. At Whakaari the conceptual model of the magmatic/hydrothermal system [Christenson et al. 2017; Miller et al. 2020] comprises single-phase gas conduits linked to shallow magma that grade radially into two-phase and finally single-phase liquid as a function of distance from the conduit. We propose that as new hot magmatic gas is injected, these single-phase gas zones expand outward and boil off any remaining liquid in the two-phase or single-phase liquid region, thereby creating pressurized steam zones. Hydrothermal sealing of the conduit via precipitation of minerals such as alunite and gypsum [Christenson et al. 2017] also aids in pressurizing the conduit.

Whakaari is described as a pulsatory gas emitter [Werner et al. 2008] that in addition to tremor, creates a range of low-frequency seismic signals associated with deep degassing through a leaky magma carapace [Jolly et al. 2018]. We suggest that repeated pulses of heat and gas from the magma carapace into overlying single-phase gas conduits create peri-

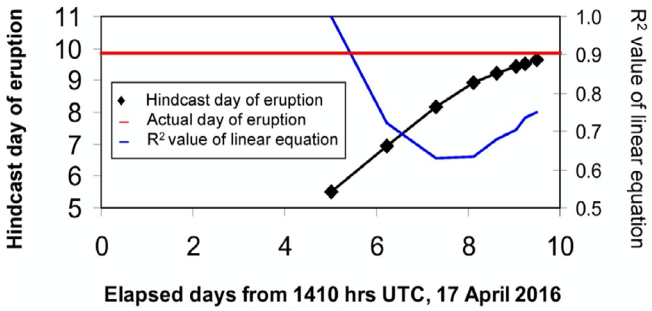


Figure 10: Plot showing hindcast day for the 27 April 2016 eruption by extrapolating linear equations forward to where $y = 0$ (the zero point). Successive linear equations are constructed for cumulative time intervals between tremor peaks, and the associated hindcast day of eruption is plotted (black diamonds). The horizontal red line shows the actual day of eruption (9.84 days) since the appearance of the first tremor peak at 1410 hours UTC on 17 April 2016. The blue line shows the changing $R^2$ values of the successive linear equations. The plot shows an increasingly accurate forecast with time.

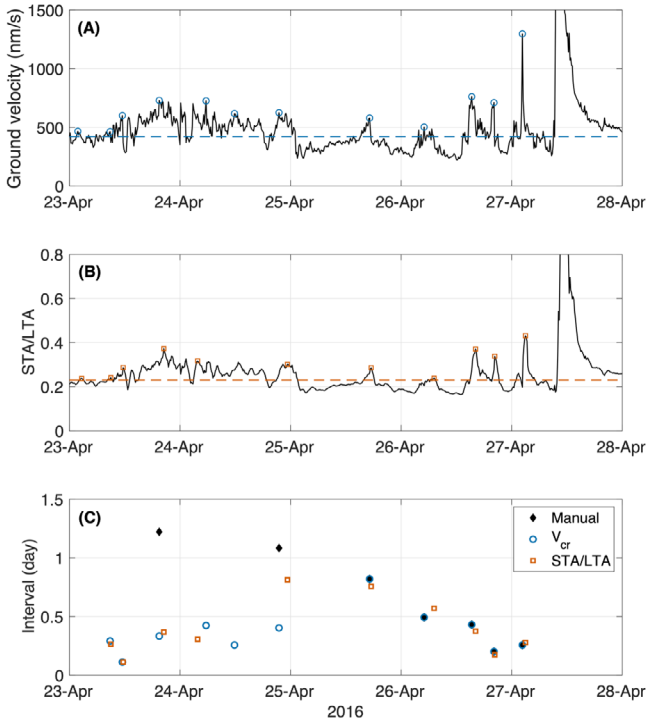


Figure 11: [A] Tremor bands selected by applying $V_{cr}$ = 420 nm s$^{-1}$, $T_{cr}$ = 0.2 days (blue circles) between 23–28 April 2016, [B] tremor bands selected by STA/LTA using short-term window of 0.01 days and long-term window of 0.05 days and a cutoff STA/LTA ratio of 0.23 (orange squares), and [C] comparison of tremor bands intervals identified from visual inspection (black diamonds, same as in Figure 9), from RSAM raw data (blue circles) and from STA/LTA ratio (orange squares).

odic boiling of the neighbouring two-phase and single-phase liquid zones, increasing overall conduit pressure. Then, at the peak of the tremor signal, the conduit is micro-fractured by the increased steam pressure causing boiling to stop and the tremor to abruptly drop. Repeated boiling and fracture cycles eventually lead to large scale failure and eruption.

For the 2019 eruption, the narrowing intervals between tremor bands were the result of increased pressurization within the hydrothermal system, with the hydrothermal system boiling more frequently as pressure built within. During the early phase of the tremor sequence, we hypothesize that pressurization rates were variable. The decreasing interval times and increasing maximum amplitudes of tremor bands within intervals #2–4 (Figure 7) are suggestive of increasing pressurization rates. From interval #6 onward, the variability declined (Figure 5), indicative of overpressures approaching and then stabilizing at a maximum value. A key difference between our model and that of Ardid et al. [2022] is that pressurization occurs at an earlier stage in our model relative to theirs.

Sulfur dioxide fluxes measured by TROPOMI satellite imagery on 26, 29, and 30 November were low and did not exceed 4 kg s$^{-1}$ [Burton et al. 2021], consistent with a system sealed by hydrothermal minerals [Heap et al. 2019; Kennedy et al. 2020; Miller et al. 2020; Mick et al. 2021]. Such highly altered materials have tensile strengths less than 7 MPa [Heap et al. 2022]; thus, the maximum overpressure was likely of similar magnitude or less. The sudden decline in amplitudes of the tremor bands beginning on 2 December suggests two scenarios. (1) At this point, boiling was no longer able to generate high pressures, indicating that the seal above the hydrothermal system started to weaken at this time due to pressure-induced fracturing accumulated with each pressurization/tremor cycle in the two weeks prior [Montanaro et al. 2022]. This point corresponds to the peak in nDSAR rate variance which Ardid et al. [2022] correlated with high gas fluxes at the surface. (2) An alternative hypothesis is that the decline in amplitudes signals higher sealing pressures that reduced boiling. The seal then remained intact until it failed catastrophically on 9 December. Seal weakening, or pressure building beneath an intact seal, continued from 2 to 9 December, at which point the pressure exceeded seal strength and the volcano erupted. The large tremor spikes observed at 17.5 and 16.2 hours prior to eruption could indicate failed or aborted eruptions [Dempsey et al. 2020]. These spikes correspond with the initiation of an inverse RSAM decline which continued until the eruption [Ardid et al. 2022]. Interestingly, the two large spikes were themselves preceded by two smaller spikes at 23.3 and 25.5 hours before the eruption. These could represent the initiation of seal failure. Such signals are termed cascading material failure by Ardid et al. [2022].

A resistivity survey of the shallow subsurface beneath the crater area at Whakaari was made in January 2019, 11 months before the 9 December eruption [Miller et al. 2020]. A laterally extensive conductive zone was mapped at depths of 20–150 m and interpreted as liquid-dominated and sealed on top [Miller et al. 2020]. Single and two-phase zones were imaged around the Fumarole 1 conduit (Figure 1), like those proposed by Christenson et al. [2017] beneath the main vent. We hypothesize that increased supply of hot magmatic fluids (gas) starting on 22 November resulted in boiling of the two-phase or liquid-dominated zones within the main vent area, generating

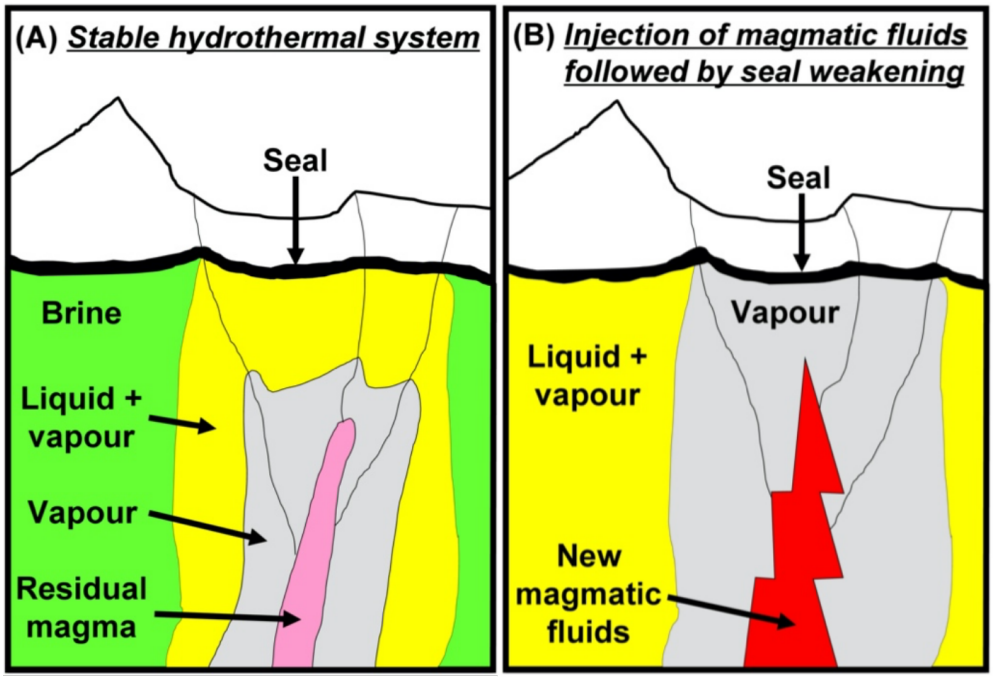


Figure 12: Conceptual representation of the Whakaari magmatic-hydrothermal system prior to the 9 December 2019 eruption, modified from Christenson et al. [2017]. [A] The hydrothermal system is stable prior to 22 November 2019. The system comprises a series of vapour, vapour plus liquid, and brine zones radiating outward from a residual magmatic core. The shallow seal is strong. [B] State of the hydrothermal system after 2 December 2019. Input of magmatic fluids has expanded the vapour zone, the system is now fully pressurized, and the seal has begun to weaken.

overpressure as liquid boiled and converted to vapour. The decreased amplitude of the tremor bands beginning on 2 December could also be explained by a third scenario whereby the bulk of the liquid was now converted to vapour in the two-phase or liquid zones. If so, this vapour-dominated and overpressured system was now primed to erupt.

A schematic view of the pre-eruptive sequence is shown in Figure 12 and summarized as follows. Prior to 22 November, the magmatic-hydrothermal system was in a state of comparative stability. Injection of magmatic fluids beginning on 22 November began to destabilize the system, with the main pressurization interval occurring from 22 November to 2 December. The seal began to fail 25.5 hours prior to the eruption, and then failed fully during the eruption on 9 December. The low tremor during the week before the eruption may indicate that: (a) seal weakening was a largely aseismic process driven by ductile failure of low-strength hydrothermally altered materials, (b) pressures below the seal were high enough to suppress boiling and hence tremor generation, and/or (c) there was no remaining liquid to boil, as it had been previously converted to vapour. The very high level of tremor for three days after the eruption may be ascribed to strong degassing and/or rise of magma through a now open conduit. $SO_2$ fluxes measured by COSPEC on 12 December three days after the eruption were elevated at 20 kg s$^{-1}$ [GeoNet 2019a], and lava was first observed in the crater on 20 January 2020 [GeoNet 2020].

Our model for the 2019 eruption can be applied to the 2016 eruption as well. The main difference between the two eruptions is the shorter time interval in 2016 between the first tremor spike and the eruption (~10 days for 2016 vs. ~17 days for 2019). This difference could indicate a shorter pressurization interval, a different magmatic input, and/or a greater degree of sealing initially. In detail, the best-defined tremor peaks for 2016 began occurring only 2.5 days before the eruption, indicating that the sequence of pressurization, seal weakening, and eruption was short. These observations suggest that the Whakaari system can reach critical pressurization thresholds and erupt on short timescales varying from days to weeks, making it difficult (but not impossible) to provide timely forecasts and warnings in the future.

## 6 Outlook and conclusions

The seismic sequences observed at Whakaari in November–December 2019 and April 2016 are important for three principal reasons. First, the sequences provide new insight into forecasting eruptions and understanding shallow subsurface processes at Whakaari, with the banded tremor serving as a harbinger to impending explosive eruptions. Second, data from both seismic stations on the island reveal a clearly decreasing interval between tremor bands, providing an accurate hindcast to within 10.2 hours of the 9 December 2019 eruption one week beforehand. The same approach provides an even better hindcast to within 2.3 hours of the 27 April 2016 eruption 14.2 hours prior. The simple approach described herein may represent a way forward to accurately forecast and even predict future eruptions at this volcano. Third, the patterns observed at Whakaari suggest multiple timescales of unrest and activity. We have shown above that the volcano

can reach critical pressurization and erupt on timescales of days to weeks. Longer eruptive patterns on the order of years could also be operating within the volcano. Since the recent unrest period began in 2011, eruptions have occurred in 2012–2013, 2016, and 2019. This hypothetical three to four-year cycle could indicate the timescale of fracture closing, mineral precipitation, and longer-term sealing processes before a critical pressurization threshold is reached.

Banded tremor is a clear indication of active pressurization within a shallow magmatic-hydrothermal system. It is also a good indicator of an impending explosive eruption. The 2016 and 2019 Whakaari data presented in this paper show that the interval between pressurization and eruption can be variable, and this variability is most likely a function of the rate and duration of the magmatic input, be it gas, heat, and/or magma. Hence the available time window for forecasting an eruption can also vary on the order of days as shown by 95 % confidence intervals. These operational details can become critical when the window is short, as seen for the 2016 eruption.

The patterns of banded tremor seen at Whakaari show certain parallels with the material failure forecast method (FFM) [Voight 1988; Voight and Cornelius 1991], as observed at a number of volcanoes. Both have "zero points" which can be used to indicate when an eruption should occur. The FFM method applies to material such as rock or magma which is being stressed and weakened. As a result, seismicity accelerates exponentially as the material fractures and breaks. This was observed at Redoubt volcano, Alaska, in 2009 as the period of both harmonic tremor and earthquakes declined prior to explosive eruptions [Hotovec et al. 2013]. In contrast, the banded tremor signals at Whakaari indicate progressive pressurization of the hydrothermal system. As the pressure builds, the signals become more frequent and their period decreases.

A key consideration is when pressurization is not followed by an eruption. This raises three crucial issues for forecasting, namely if a volcano will erupt, when it will erupt, and how big the eruption will be. While the issues of if and how big remain significant challenges for future work, here we have shown through a detailed retrospective analysis some useful relationships in regards to when. A systematic search for similar precursory signals and patterns of decreasing banded tremor intervals are needed to help recognize global patterns, in particular at volcanoes with well-developed hydrothermal systems. Another interesting question for future studies is to investigate whether similar patterns are present or not during periods of elevated tremor but no eruptions.

The utility of this potential forecasting approach may be applicable to other volcanoes which behave similarly to Whakaari. Such volcanoes can have magma residing at shallow levels beneath the volcano and may reach critical pressurization thresholds over short time periods. They generally have well-developed hydrothermal systems, and subsurface magmatic-hydrothermal interactions are common. Eruption styles include phreatic, phreatomagmatic, and magmatic. To date, it has not been possible to forecast or predict sudden eruptions from these types of volcanoes. The analysis presented in this paper may offer a new step forward toward this goal.

## Author Contributions

Conceptualisation: JS. Formal Analysis: JA, CM, YL. Investigation: JS, CM. Methodology: JS, CM. Validation: YL. Visualisation: JS, YL. Writing original draft: JS. Writing review and editing: CM, YL.

## Acknowledgements

We acknowledge the New Zealand GeoNet project and its sponsors EQC, GNS Science, LINZ, NEMA, and MBIE for data shown in Figures 1, 2, 3 and 8. We thank Art Jolly, Alberto Ardid, and Corentin Caudron for very helpful reviews and comments which improved the paper. Jamie Farquharson and Oliver Lamb provided extremely useful suggestions on an earlier version of the manuscript. We are also grateful to Bruce Christenson for insightful comments. We thank Justin Chien for assistance with spectral analysis. JS acknowledges ongoing financial support from the Natural Sciences and Engineering Research Council of Canada in the form of a Discovery Grant (RGPIN-2020-04197) which helped support this work. CM is funded by the New Zealand Government Ministry of Business, Employment and Innovation through the Strategic Science Investment Fund and through the Endeavour Research Programme Beneath the Waves (contract C05X2102). YL is supported by the Natural Sciences and Engineering Research Council (NSERC) Discovery Grant RGPPIN-2018-05389.

## Data Availability

All data are available in the paper. Raw seismic data are available from GeoNet via https://www.geonet.org.nz/data/access/FDSN.

## Copyright Notice



## References

Ardid, A., D. Dempsey, C. Caudron, and S. Cronin (2022). "Seismic precursors to the Whakaari 2019 phreatic eruption are transferable to other eruptions and volcanoes". *Nature Communications* 13(2002). DOI: 10.1038/s41467-022-29681-y.

Banks, N. G., R. I. Tilling, D. H. Harlow, and J. W. Ewert (1989). "Volcano monitoring and short-term forecasts". *Volcanic Hazards*. Volume 1. American Geophysical Union Washington, DC, pages 81–102. DOI: 10.1029/SC001p0051.

Barberi, F., A. Bertagnini, P. Landi, and C. Principe (1992). "A review on phreatic eruptions and their precursors". *Journal of Volcanology and Geothermal Research* 52(4), pages 231–246. DOI: 10.1016/0377-0273(92)90046-G.

Burton, M., C. Hayer, C. Miller, and B. Christenson (2021). "Insights into the 9 December 2019 eruption of Whakaari/White Island from analysis of TROPOMI $SO_2$ imagery". *Science Advances* 7(eabg1218). DOI: 10.1126/sciadv.abg1218.

Chardot, L., A. D. Jolly, B. M. Kennedy, N. Fournier, and S. Sherburn (2015). "Using volcanic tremor for eruption forecasting at White Island volcano (Whakaari), New Zealand". *Journal of Volcanology and Geothermal Research* 302, pages 11–23. DOI: 10.1016/j.jvolgeores.2015.06.001.

Christenson, B., S. White, K. Britten, and B. Scott (2017). "Hydrological evolution and chemical structure of a hyper-acidic spring-lake system on Whakaari/White Island, NZ". *Journal of Volcanology and Geothermal Research* 346, pages 180–211. DOI: 10.1016/j.jvolgeores.2017.06.017.

Cole, J., T. Thordarson, and R. Burt (2000). "Magma origin and evolution of White Island (Whakaari) volcano, Bay of plenty, New Zealand". *Journal of Petrology* 41(6), pages 867–895. DOI: 10.1093/petrology/41.6.867.

Dempsey, D., S. J. Cronin, S. Mei, and A. W. Kempa-Liehr (2020). "Automatic precursor recognition and real-time forecasting of sudden explosive volcanic eruptions at Whakaari, New Zealand". *Nature Communications* 11(3562). DOI: 10.1038/s41467-020-17375-2.

Dempsey, D., A. Kempa-Liehr, A. Ardid, A. Li, S. Orenia, J. Singh, A. Tyler, and S. Cronin (2022). "Evaluation of short-term probabilistic eruption forecasting at Whakaari, New Zealand". *Bulletin of Volcanology* 84(91). DOI: 10.1007/s00445-022-01600-5.

GeoNet (2019a). *GeoNet Volcanic Alert Bulletin WI-2019/28 – Whakaari/White Island: update #16*. URL: https://geonet.org.nz/vabs/22jPzcEJrg7jxxZf0By7ty.

– (2019b). *Whakaari/White Island likelihood of future eruption: update #2*. URL: https://www.geonet.org.nz/news/60xDrUB7wRZPZXyBa8xYwE.

– (2020). *GeoNet Volcanic Alert Bulletin WI-2020/03 – Whakaari/White Island: update #20*. URL: https://www.geonet.org.nz/vabs/4gbGrPpouFsu3Sy045QLrs.

GNS Science (2021). "GeoNet Aotearoa New Zealand Seismic Digital Waveform Dataset". *GNS Science, GeoNet*. DOI: 10.21420/G19Y-9D40. [Dataset].

Gresta, S., E. Privitera, A. Leotta, and P. Gasperini (1996). "Analysis of the intermittent volcanic tremor observed at Mt. Etna, Sicily during March–May 1987". *Annals of Geophysics* 39(2), pages 421–428.

Heap, M. J., C. E. Harnett, F. B. Wadsworth, H. A. Gilg, L. Carbillet, M. Rosas-Carbajal, J.-C. Komorowski, P. Baud, V. R. Troll, F. M. Deegan, E. Holohan, and R. Moretti (2022). "The tensile strength of hydrothermally altered volcanic rocks". *Journal of Volcanology and Geothermal Research* 428(107576). DOI: 10.1016/j.jvolgeores.2022.107576.

Heap, M. J., V. R. Troll, A. R. Kushnir, H. A. Gilg, A. S. Collinson, F. M. Deegan, H. Darmawan, N. Seraphine, J. Neuberg, and T. R. Walter (2019). "Hydrothermal alteration of andesitic lava domes can lead to explosive volcanic behaviour". *Nature Communications* 10(5063). DOI: 10.1038/s41467-019-13102-8.

Hotovec, A. J., S. G. Prejean, J. E. Vidale, and J. Gomberg (2013). "Strongly gliding harmonic tremor during the 2009 eruption of Redoubt Volcano". *Journal of Volcanology and Geothermal Research* 259, pages 89–99. DOI: 10.1016/j.jvolgeores.2012.01.001.

Houghton, B. and I. Nairn (1991). "The 1976–1982 Strombolian and phreatomagmatic eruptions of White Island, New Zealand: eruptive and depositional mechanisms at a 'wet' volcano". *Bulletin of Volcanology* 54, pages 25–49. DOI: 10.1007/BF00278204.

Jolly, A., C. Caudron, T. Girona, B. Christenson, and R. Carniel (2020). "'Silent' dome emplacement into a wet volcano: observations from an effusive eruption at White Island (Whakaari), New Zealand in late 2012". *Geosciences* 10(142). DOI: 10.3390/geosciences10040142.

Jolly, A., I. Lokmer, B. Christenson, and J. Thun (2018). "Relating gas ascent to eruption triggering for the April 27, 2016, White Island (Whakaari), New Zealand eruption sequence". *Earth, Planets and Space* 70(177). DOI: 10.1186/S40623-018-0948-8.

Kennedy, B. M., A. Farquhar, R. Hilderman, M. C. Villeneuve, M. J. Heap, S. Mordensky, G. Kilgour, A. Jolly, B. Christenson, and T. Reuschlé (2020). "Pressure controlled permeability in a conduit filled with fractured hydrothermal breccia reconstructed from ballistics from Whakaari (White Island), New Zealand". *Geosciences* 10(138). DOI: 10.3390/geosciences10040138.

Kilgour, G., B. Kennedy, B. Scott, B. Christenson, A. Jolly, C. Asher, M. Rosenberg, and K. Saunders (2021). "Whakaari/White Island: a review of New Zealand's most active volcano". *New Zealand Journal of Geology and Geophysics* 64(2-3), pages 273–295. DOI: 10.1080/00288306.2021.1918186.

Martinelli, B. (1990). "Analysis of seismic patterns observed at Nevado del Ruiz volcano, Colombia during August–September 1985". *Journal of Volcanology and Geothermal Research* 41(1-4), pages 297–314. DOI: 10.1016/0377-0273(90)90093-U.

McKee, C., D. Wallace, R. Almond, and B. Talai (1981). "Fatal hydro-eruption of Karkar volcano in 1979: Development of a maar-like crater". *Cooke-Ravian Volume of Volcanological Papers*. Volume 10. Geological Survey of Papua New Guinea Port Moresby, Papua New Guinea, pages 63–84.

Meng, H. and Y. Ben-Zion (2018). "Characteristics of airplanes and helicopters recorded by a dense seismic array near Anza California". *Journal of Geophysical Research: Solid Earth* 123(6), pages 4783–4797. DOI: 10.1029/2017JB015240.

Mick, E., J. Stix, J. M. de Moor, and G. Avard (2021). "Hydrothermal alteration and sealing at Turrialba volcano, Costa Rica, as a mechanism for phreatic eruption triggering". *Journal of Volcanology and Geothermal Research* 416(107297). DOI: 10.1016/j.jvolgeores.2021.107297.

Miller, C. A., B. W. Christenson, S. Byrdina, J. Vandemeulebrouck, T. Brakenrig, K. Britten, J. Shanks, and G. Epstein (2020). "Snapshot of a magmatic/hydrothermal system from electrical resistivity tomography and fumarolic composition, Whakaari/White Island, New Zealand". *Journal of Volcanology and Geothermal Research* 400(106909). DOI: 10.1016/j.jvolgeores.2020.106909.

Montanaro, C., E. Mick, J. Salas-Navarro, C. Caudron, S. J. Cronin, J. M. de Moor, B. Scheu, J. Stix, and K. Strehlow (2022). "Phreatic and hydrothermal eruptions: from overlooked to looking over". *Bulletin of Volcanology* 84(64). DOI: 10.1007/s00445-022-01571-7.

Stix, J. and J. M. de Moor (2018). "Understanding and forecasting phreatic eruptions driven by magmatic degassing". *Earth, Planets and Space* 70(83). DOI: 10.1186/s40623-018-0855-z.

Vandemeulebrouck, J., D. Stemmelen, T. Hurst, and J. Grangeon (2005). "Analogue modeling of instabilities in crater lake hydrothermal systems". *Journal of Geophysical Research: Solid Earth* 110(B02212) (B2). DOI: 10.1029/2003JB002794.

Voight, B. (1988). "A method for prediction of volcanic eruptions". *Nature* 332, pages 125–130. DOI: 10.1038/332125a0.

Voight, B. and R. R. Cornelius (1991). "Prospects for eruption prediction in near real-time". *Nature* 350, pages 695–698. DOI: 10.1038/350695a0.

Werner, C., T. Hurst, B. Scott, S. Sherburn, B. Christenson, K. Britten, J. Cole-Baker, and B. Mullan (2008). "Variability of passive gas emissions, seismicity, and deformation during crater lake growth at White Island Volcano, New Zealand, 2002–2006". *Journal of Geophysical Research: Solid Earth* 113(B01204) (B1). DOI: 10.1029/2007JB005094.

Yamaoka, K., N. Geshi, T. Hashimoto, S. E. Ingebritsen, and T. Oikawa (2016). "Special issue "The phreatic eruption of Mt. Ontake volcano in 2014"". *Earth, Planets and Space* 68(1), page 175. DOI: 10.1186/s40623-016-0548-4.